





Lightsheet-based flow cytometer for whole blood with the ability for the magnetic retrieval of objects from the blood flow

ROMAN A. VERKHOVSKII,¹ ANASTASIIA A. KOZLOVA,¹ OLGA A. SINDEEVA,^{1,2} ILYA O. KOZHEVNIKOV,¹ EKATERINA S. PRIKHOZHDENKO,¹ OKSANA A. MAYOROVA,¹  OLEG V. GRISHIN,¹ MIKHAIL A. MAKARKIN,¹ ALEXEY V. ERMAKOV,¹ ARKADY S. ABDURASHITOV,²  VALERY V. TUCHIN,^{1,3,4}  AND DANIIL N. BRATASHOV^{1,*} 

¹Saratov State University, 83 Astrakhanskaya str., Saratov 410012, Russia

²Skolkovo Innovation Center, 3 Nobel str., Moscow 121205, Russia

³National Research Tomsk State University, 36 Lenin Avenue, Tomsk 634050, Russia

⁴Institute of Precision Mechanics and Control of the RAS, 24 Rabochaya str., Saratov 410028, Russia

*dn2010@gmail.com

Abstract: Detection and extraction of circulating tumor cells and other rare objects in the bloodstream are of great interest for modern diagnostics, but devices that can solve this problem for the whole blood volume of laboratory animals are still rare. Here we have developed SPIM-based lightsheet flow cytometer for the detection of fluorescently-labeled objects in whole blood. The bypass channel between two blood vessels connected with the external flow cell was used to visualize, detect, and magnetically separate fluorescently-labeled objects without hydrodynamic focusing. Carriers for targeted drug delivery were used as model objects to test the device performance. They were injected into the bloodstream of the rat, detected fluorescently, and then captured from the bloodstream by a magnetic separator prior to filtration in organs. Carriers extracted from the whole blood were studied by a number of *in vitro* methods.

© 2020 Optical Society of America under the terms of the [OSA Open Access Publishing Agreement](#)

1. Introduction

Direct analysis of rare pathogens and embolus in the blood flow should provide extremely important capabilities for the next generation of diagnostic systems. This task is essential for both diagnostic purposes and pre-clinical testing of modern therapy methods. Circulating tumor cells (CTCs) in the case of metastatic cancers [1,2]; microorganisms [3] and protozoa [4] during blood infections; atherosclerotic plaques [5] and red blood cell clots during cardiovascular diseases [6] can be detected by direct measurement of patients' blood. But in the early disease stages, when the detection of such objects is extremely important, the possibility of doing so is utterly low. Thus, the major challenge of modern diagnostics is the detection of such rare events in the patient's whole blood. In therapy, it can be applied for thorough comprehensive pre-clinical testing of novel methods, especially based on targeted drug delivery platforms.

Currently, several approaches for *in vivo* detection and separation of such objects have been developed. At first glimpse, a search for rare cells in the blood flow and investigation of processes between numerous drug delivery carriers have completely different engineering requirements. However, the sensitivity of the system designed to detect single objects in a large amount of blood cells provides necessary reliability for the complex testing of drug delivery systems. On the other hand, a large number of circulating carriers for targeted drug delivery with well-defined parameters can be detected much more easily than single unique objects with unknown features. Moreover, testing of the system using well-characterized objects greatly simplifies its development.

Large amounts of blood should be analyzed in order to capture CTCs at the early stages of cancer, or specific pathogen germs at the beginning of acute blood infection. According to the literature, the amount of CTCs contained in 1 mL of whole blood can range from a few to several hundred objects depending on the cancer stage and correlates with the disease progression [7,8]. Meanwhile, the typical pathogen germs concentration during sepsis is approximately 10^3 colony-forming units (CFU)/mL in blood samples [9]. Moreover, no objects of interest may be captured into the blood sample, which conventional size is 7.5 mL [10,11], as there are fluctuations in the rate of objects appearance in circulation [12,13].

In vivo cytometry systems overpass this restriction by the analysis of the total volume of whole blood. In combination with photoacoustic microscopy, such systems can be applied for early malaria diagnostics [4], detection of circulating melanoma cells [14,15], and other kinds of emboli [16]. However, their functioning in most cases is provided by the characteristic features inherent in the objects of interest. For instance, such features can be a high optical absorbance and a specific spectrum for circulating melanoma cells, providing their *in vivo* photoacoustic flow cytometry detection. In other cases, such features should be created by cells labeling directly in the blood flow *in vivo* with following photoacoustic [17] or fluorescent [10,18,19] detection.

Another possible way to search for rare objects in a large volume of blood is based on the imaging flow cytometry. Various approaches have used 3D detection capabilities for imaging flow cytometry and have reduced the need for hydrodynamic focusing, which requires diluting whole blood with the sheath fluid. They include lightsheet scheme of SPIM-Fluid device [20], line-field quantitative phase microscopy with digital refocusing [21], orthogonal light-sheet scanning illumination with spatiotemporal transformation detection producing 3D cell image reconstruction from a cameraless single-pixel photodetector readout [22], virtual-freezing fluorescence imaging flow cytometry [23], and other schematics.

Despite all the advantages of non-invasive *in vivo* flow cytometry, it has one significant drawback — the inability to retrieve the analyzed objects from the bloodstream for further additional research. The most mature approach to solve this problem is the extracorporeal separation of such objects from the flow of whole blood. Magnetically-labeled objects [24–26] can be trapped from the blood flow using the magnetic separator [27–30] integrated with the flow cell. Systems for the magnetic separation of objects from the patient's blood pumped by an additional peristaltic pump are being actively developed now [31]. The main purpose of such devices is the cleaning of blood from pathological cells labeled by functionalized magnetic beads.

Our approach is based on a combination of two methods. The first is the visualization of fluorescent objects in undiluted blood performed in the external flow cell by the lightsheet system based on SPIM-Fluid design. The second is the separation of magnetically-labeled objects using a permanent rare-earth magnet with concentrator, similar to the one used in our previous studies [25,26]. This approach combines the advantages of an *in vivo* flow cytometer, which analyzes the entire blood volume with detection of rare objects, and a magnetic cell sorter, which captures magnetically-labeled objects from the bloodstream. In addition, this technical solution does not require focusing the object flow in the caustic region of the laser and focusing the camera, which allows working directly with undiluted blood and performing flow cytometry measurements in a flow cell that connects two blood vessels of a laboratory animal. The external flow cell eliminates the scattering and attenuation of laser radiation by biological tissues and their autofluorescence compared to *in vivo* cytometry. Technology approbation was performed both *in vitro* and *in vivo* using the biodegradable fluorescently-labeled magnetic capsules as model objects.

2. Material and methods

2.1. Materials

Dextran sulfate sodium salt (DS, MW>70 000), fluorescein isothiocyanate (FITC), poly-L-arginine hydrochloride (pArg, MW>70 000), bovine serum albumin (BSA), phosphate-buffered

saline (PBS, 0.01 M), calcium chloride dihydrate, anhydrous sodium carbonate, sodium chloride, ethylenediaminetetraacetic acid disodium salt (EDTA), iron (III) chloride (FeCl_3), iron (II) chloride (FeCl_2), citric acid were obtained from Sigma-Aldrich, dimethyl sulfoxide (DMSO), sodium hydroxide were obtained from Merck and used without further purification.

2.2. Device design

The optical design of the device is based on a simplified variant of the SPIM-Fluid imaging flow cytometer [20]. The major features are shown in Fig. 1. The device is composed of three main units:

- *a light-sheet illumination subsystem* that consists of CW diode lasers: 488 nm 60 mW (Cobolt MLD 06-01, Hübner Photonics, Germany), 561 nm 50 mW (Cobolt DPL, Hübner Photonics, Germany), 660 nm 100 mW (Cobolt 06-MLD, Hübner Photonics, Germany); delivery of laser light and beams collimation from several sources is done by periscopes formed for each laser either by the pair of silver mirrors (M) (PF10-03-P01, Thorlabs, USA) or pair of silver and dichroic mirrors (DM) (DMLP505 or DMLP605, Thorlabs, USA); 3.5× beam expander (formed by pair of lenses: LA1131-A and LA1229-A, Thorlabs, USA); and light-sheet generation telecentric system that consists of a cylindrical lens (CL) ($f = 50$ mm, LJ1695RM-A, Thorlabs, USA) and an objective (MO_{LS} , 4×, NA = 0.13, CFI Plan Fluor, Nikon, Japan). The focus of the lightsheet beam is adjusted using a PT1/M stage (Thorlabs, USA).
- *an image detection subsystem* that consists of an objective (MO, 10×, NA = 0.3, CFI Plan Fluor, Nikon, Japan), a fluorescence imaging filters kit (MF530-43 — FITC Emission Filter; MF620-52 — TRITC/CY3.5 Emission Filter, Thorlabs, USA) in a custom-made motorized filter wheel based on FW1AB (Thorlabs, USA), a tube lens (TL, $f = 200$ mm, LBF254-200-A, Thorlabs, USA), and Monochrome CMOS Camera (CS505MU, Thorlabs, USA). The focus is adjusted using a PT1/M stage (Thorlabs, USA).
- *a flow subsystem* that consists of a flow cell based on UV Quartz clear flow-through cuvette (526UV0.25, FireflySci, US), permanent rare earth magnet with a homemade magnetic field concentrator that provides a magnetic field strength of 0.3 T in the position of the flow channel near the end of the concentrator, if the magnet is brought to flow cell. The magnet moves along the channel using the MS1S/M stage (Thorlabs, USA). The magnetic field parameters were measured by the SJ200 hand-held digital Gauss meter with the Hall sensor. The flow cell can be connected by plastic tubing either with the syringe pump AL-1000 (World Precision Instruments, USA) and 50 mL tube used as waste or with the catheters connected directly to the laboratory animal blood flow.

2.3. Synthesis of test objects

2.3.1. Synthesis of citrate-stabilized magnetite nanoparticles

Magnetite nanoparticles (MNPs) were synthesized by chemical precipitation method from di- and trivalent iron salts into an alkaline media as described before [32,33]. Initially, 1.3 g of $\text{FeCl}_3 \cdot 6\text{H}_2\text{O}$ and 0.478 g of $\text{FeCl}_2 \cdot 4\text{H}_2\text{O}$ were dissolved in 25 mL of water under room temperature with mixing. 170 mL of 0.1 M NaOH was added to the reaction cell. Further colloids stabilization was made by 25 mL of citric acid (32 mg/mL) aqueous solution. Nitrogen was bubbled through the closed cell with a mixture of iron salts, sodium hydroxide, and citric acid for 10 min to remove excess oxygen from the solution. After that, the sodium hydroxide solution was heated to 40°C, the solution of iron salts solutions were introduced into the reaction cell with vigorous stirring, after which the solution was left under vigorous stirring and nitrogen

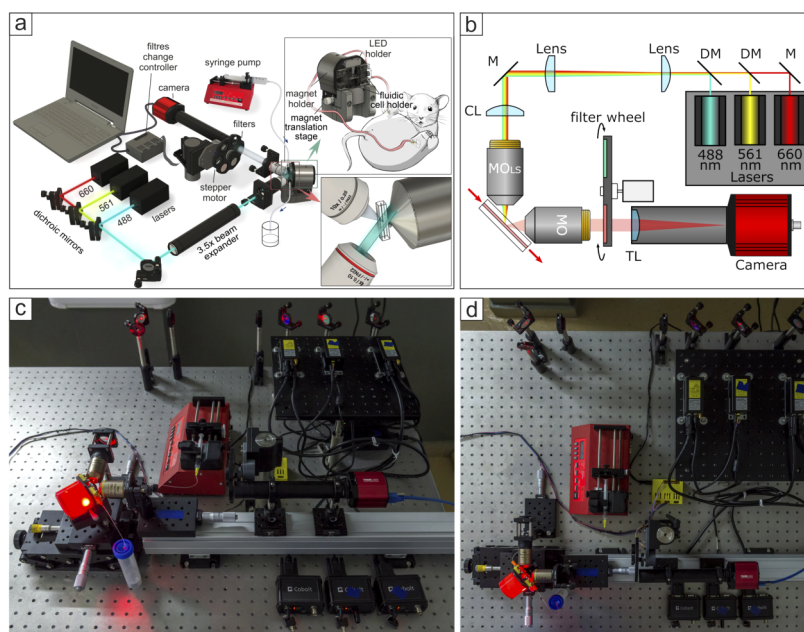


Fig. 1. Overall system design (a), optical schematics (b), and photos (c and d) of the device combining lightsheet-based cytometer and magnetic separator of objects. M — mirror; DM — dichroic mirror; CL — cylindrical lens; MO_{LS} — lightsheet forming microobjective; MO — detection subsystem microobjective; TL — tube lens.

pressure for 40 s, as a result of which a black sediment of magnetite nanoparticles was formed. Then the citric acid solution was added to the suspension under constant stirring and nitrogen pressure. Dialysis of the resulting magnetic hydrosol was performed during 3 days in 3 L vial under slow mixing. Mixing of reagents and washing were performed under nitrogen atmosphere.

2.3.2. Synthesis of FITC-labeled BSA

First, 160 mg of BSA were dissolved in 40 mL of 0.1 M PBS buffer (pH 8). Afterward, the solution of FITC in ethanol (5 mg/mL) was prepared. 40 mL of BSA solution was added to 5 mL of FITC alcoholic solution under gentle stirring and the mixture was left with constant steering under 4°C in the dark for 12 h. Finally, freshly prepared FITC-conjugated BSA was dialyzed for 3 days in deionized water.

2.3.3. Preparation of fluorescent magnetic microcapsules

Spherical porous $CaCO_3$ particles (average size of ~ 0.8 – $1.2 \mu m$) with the co-precipitated MNPs were synthesized similarly to that described earlier [34]. In brief, 0.4 mL of 0.5 M $CaCl_2$ and 0.5 M Na_2CO_3 solutions were injected into 4 mL of glycerol and 2 mL of MNP suspension under vigorous stirring. One hour later stirring was stopped, the particle suspension was centrifuged and washed two times by deionized water.

Layer-by-Layer assembly was used to obtain microcarriers. Microcapsules were formed by the sequential adsorption of 1 mL of pArg (1 mg/mL), DS (1 mg/mL), and BSA-FITC (1 mg/mL) from 0.15 M NaCl solutions onto the surfaces of the spherical $CaCO_3$ cores. The cores were then dissolved with EDTA (pH 7.3). The obtained shell structure was $[MNPs/pArg/DS/\{pArg/BSA-FITC\}_2/pArg/DS]$.

2.4. *In vitro and in vivo experiments*

2.4.1. *In vitro* experiments

During *in vitro* study, the fluorescent magnetic capsules suspended in PBS or in the rat blood (the ratio of blood to capsule PBS suspension was 3:1) were used as test samples. The flow cell was connected to two tubes, one connected to a constant flow syringe pump and the other to a waste container.

2.4.2. Laboratory animal experiment *in vivo*

Animal care and all experimental procedures were carried out in accordance with the "Guide for the Care and Use of Laboratory Animals" [35]. For general animal anesthesia, the mix of Zoletil solution in the concentration of 40 mg/kg (Virbac SA, Carros, France) and 2% Rometar in the concentration of 10 mg/kg (Spofa, Czech Republic) was injected intraperitoneal. The experimental protocol was approved by the Committee for the Care and Use of Laboratory Animals at Saratov State Medical University (wide approval no. 5 on 29.12.2018). The study was carried out on adult male white mongrel rats with an average weight of 200–250 g.

The microcapsule suspension was injected into the branch of the carotid artery (about 0.5 mm in diameter) through a thin polyethylene tube (inner diameter 0.28 mm, outer diameter 0.61 mm, Portex, Smiths Medical International Ltd., UK). Prior to the implantation, the tube was filled with isotonic NaCl (0.15 M) aqueous solution. Before injection, the capsules were also transferred into 0.15 M NaCl aqueous solution and diluted 3 times to prevent blockage of circulation due to their aggregation. The total injection volume was 20 μ L.

Evaluation of blood flow velocity The blood flow velocity in large vessels of laboratory rats was measured by the optical coherence tomography (OCT) method using Thorlabs PSOC1300SS system (Thorlabs, USA) in the Doppler measurement mode. The transverse and axial resolution of the system were 20 and 5 μ m, respectively. The A-scan rate of the system was set to 16 kHz. To ensure sufficient spatial sampling for both veins and arteries, 2048 A-scans were performed over a 5 mm section. The angle between the velocity vector and the probing beam was set to 12 degrees. The phase difference between two adjacent A-scans was used to calculate blood flow values. Due to the nature of *arctan* function, reconstructed phase values were limited by the $[-\pi, \pi]$ interval. A built-in NumPy function *unwrap* was used to unwrap the phase values thus making them usable for blood flow velocity calculation. The blood flow velocity measurement was performed on the femoral artery and vein of the right hind paw of the laboratory animal. In the area of femoral vessels, a small skin dissection was performed to provide better visualization quality (see Fig. S1 in Supplement 1).

Magnetic separation from the blood flow For the *in vivo* experiment, the input tube was connected to the femoral artery and output to the femoral vein of the rat's hind paws by catheters with an internal diameter of 0.28 mm (Fine Bore Polythene Tubing, Portex, USA). All inner surfaces of the flow channel were treated with heparin to prevent blood coagulation. Before the connection of catheters with blood vessels, all volume of the fluidic system was filled with the physiological salt solution to prevent air embolism.

In the first step, the flow cell was connected to the artery to ensure the blood pressure is enough for the blood to flow through the channel. Next, the output tube was connected to another paw's vein to provide the blood flow through the flow cell. Before and during the experiment, small portions of the heparin solution were injected through an implanted catheter into the left carotid artery to prevent thrombosis. Subsequently, the same catheter was used to inject capsules' suspension.

The capture of magnetic FITC-labeled microcapsules from the bloodstream was performed by 0.3 T magnet during 10 min. Then, the flow cell was disconnected from the rat's vascular system, the magnet was removed, and trapped capsules were collected into the tube by washing the flow channel with PBS. Finally, the 50-times diluted sample of blood containing captured

capsules was obtained and studied using the imaging flow cytometer Amnis ImageStream X MkII (Luminex, USA).

2.5. *Data processing*

2.5.1. Detecting average fluorescence in the lightsheet plane

The first and one of the simplest detection methods is based on the calculation of the average fluorescence within the region of interest (ROI) representing a lightsheet plane crossing the square capillary. If a large number of objects are simultaneously present in the image frame as a non-resolvable cluster, the average fluorescence value fairly well represents the amount of the fluorescent material in this cluster. For instance, this method performs well for analyzing fluorescent signals in the region directly alongside the tip of the magnetic concentrator in the case of numerous fluorescent magnetic objects in the sample flow. In this case, if there is a large accumulation of indistinguishable objects, the intensity of the fluorescent signal within the ROI can give an estimate of their number even if the fluorescent signal is nonlinearly dependent on the number of objects.

2.5.2. Analysis by computer vision methods

The second detection approach is based on the identification of object contours against the background. The applicability of this method depends on several characteristics of the video stream of the object flow. First, the presence of a uniform background against which the objects of interest are clearly distinguishable. Second, all counted objects belong to the same class, other types of objects are not visible in the frame (thus, there is no need for an additional classification task). Third, these objects have the same simple shape (elongated ellipsoidal contour). Fourth, the frame rate during shooting (33 frames per second) and the rapid unidirectional movement of objects in the fluid flow ensures that in the absence of a magnet, the same object will occur in one or two frames and then disappear.

There are two cases in the video stream analysis: each object is clearly separated from the others, and clusters of aggregated objects forming large nonseparable regions are present. Therefore, if the objects do not stick together in the video, we can find all the contours in a separate frame and calculate their areas using the corresponding functions of the OpenCV library. Based on the values of these areas, we evaluate the average area of the contour corresponding to a single object. Then, we subtract adjacent frames to reveal moving objects and count their number by the number of contours (one contour per object). If object adhesion is present, we determine the area of bright spot representing several objects sticking together and divide it by the calculated average contour area of a single object. Since the areas of the spots change in proportion to the number of adhering (or washed off) objects, it allows us to approximately calculate the number of objects in the frame. Despite simplicity, these algorithms show high accuracy in object counting. This was validated by the video obtained from the sample with a known number of objects. The algorithms have found 89–93% of objects depending on the presence of object agglomeration. A lower detection rate is observed in the presence of one or more large bright spots since the calculation through the average object area is inevitably less accurate. However, the results obtained here using computer vision methods correlate with the results obtained by measuring the average intensity in the lightsheet plane.

2.6. *Characterization of objects*

2.6.1. Atomic force microscopy

Atomic force microscopy (AFM) topography images of microcapsules before injection and captured from the rat blood were obtained using NTEGRA Spectra microscope (NTMDT-SI, Russia) and NSG10 tips (TipsNano, Russia) in tapping mode. All samples were dried on a glass

substrate and measured in a completely dried state. All image processing, measurements of microcapsule parameters, and correction of AFM artifacts were done using Gwyddion software [36].

2.6.2. Confocal laser scanning microscopy

Fluorescence images of microcapsules captured from the whole blood were obtained using a confocal laser scanning microscope (CLSM) Leica TCS SP8 X (Leica Microsystems, Wetzlar, Germany).

2.6.3. Flow cytometry

Captured magnetic capsules were counted and their optical properties were evaluated using the imaging flow cytometer Amnis ImageStream X Mk II. As shown in previous works [37,38], fluorescence intensity of FITC-labeled capsules does not overlap with the autofluorescence intensity of blood cells, which allows us to separate capsules from cells by fluorescence intensity gating in the range of 480–560 nm. Fluorescent dye was excited by a 488 nm laser at 100 mW power. Flow cytometry data were processed using IDEAS software (Luminex, USA).

3. Results and discussion

We have developed a SPIM-based flow cytometry system capable of visualizing objects in the flow of whole blood without dilution or hydrodynamic focusing. The flow cell of our system can be connected directly to the blood flow by shunting two large vessels in the animal's paw. It can also provide on-demand magnetic separation of objects from the flow using a rare earth permanent magnet with their following extraction.

To test the capabilities of the developed system, we used the polyelectrolyte microcapsules, functionalized with magnetite nanoparticles and labeled with FITC-BSA, as test objects. Polyelectrolyte microcapsules, in general, are well-suitable from the different points of view: they are biocompatible and do not significantly affect normal blood flow [38]; can be easily functionalized by different agents providing fluorescent [39,40], Raman [41], or photoacoustic [42,43] modalities of contrast. The microcapsules that were used in our experiments have well-defined fluorescent properties, size, and good magnetic separation ability. These hollow microcapsules were formed using CaCO_3 microparticles as templates followed by dissolution of the cores. According to AFM data, the microcapsule shell thickness was about 33 nm, and the average diameter of the capsules was $1.34 \pm 0.23 \mu\text{m}$, which was also confirmed by CLSM measurements.

Two main methods of image processing were employed to analyze data from the developed SPIM-based flow cytometry system. The raw video stream of the lightsheet and surrounding area was captured by the sCMOS camera. The first analysis method is somewhat similar to traditional fluorescence flow cytometry, which measures average fluorescence intensity inside the ROI covering all the lightsheet plane cross-section of the flow channel. The average fluorescence intensity was calculated and used as flow cytometry channel values. This method works well if objects cannot be separated due to their high concentration or aggregation in the area near the tip of the magnetic field concentrator. But signals, in this case, can be affected by the fluorescence quenching, fluorescent background of the flow, and extinction of light by the media in the flow cell. However, in general, it is still proportional to the amount of fluorescent material in the lightsheet plane. The second analysis method is based on object separation against the background followed by counting various shape parameters. This method uses the difference between two adjacent camera frames to find the background and objects visible on it, even in difficult cases of blurry images and high background fluorescence typical of blood. While working with objects of known size and shape (for example, polyelectrolyte microcapsules), small aggregates can still be separated by measuring the object's area on the image plane. It is generally similar to imaging flow cytometry data processing. However, the same objects can be detected in several planes if

the camera speed is high enough and the flow rate is low, but in our case this problem does not arise. Optical flow methods should probably be applied if a higher-speed camera is used in the experiment.

3.1. Magnetic microcapsule separation from the PBS solution

We carried out several control experiments to test the capabilities of the developed system. The first one was performed to test the magnetic microcapsule separation from PBS at different flow rates. The suspension of microcapsules in PBS buffer media was pumped through the flow cell and visualized in the lightsheet plane. Then the magnet was placed near the channel and the carriers' capture in the strong magnetic field area was registered. Due to high capsules' aggregation in the magnet tip area, we used the average level of fluorescence to detect objects. At the same time, the video of the flow was also recorded for further analysis by computer vision methods. The estimated amount of fluorescent microcapsules can be converted to a dose of a biologically active substance accumulated in the region of a strong magnetic field and extracted from the liquid flow. After registration, the magnet was removed and the desorption of carriers from the accumulation area was observed.

The velocity of the flow affects the processes of magnetic accumulation and separation of objects (Fig. 2). The magnetic field distribution from the top of the concentrator tip (in the direction perpendicular to the flow cell channel) is shown in Fig. 3(a). The field was 0.3 T measured at a distance corresponding to the channel position.

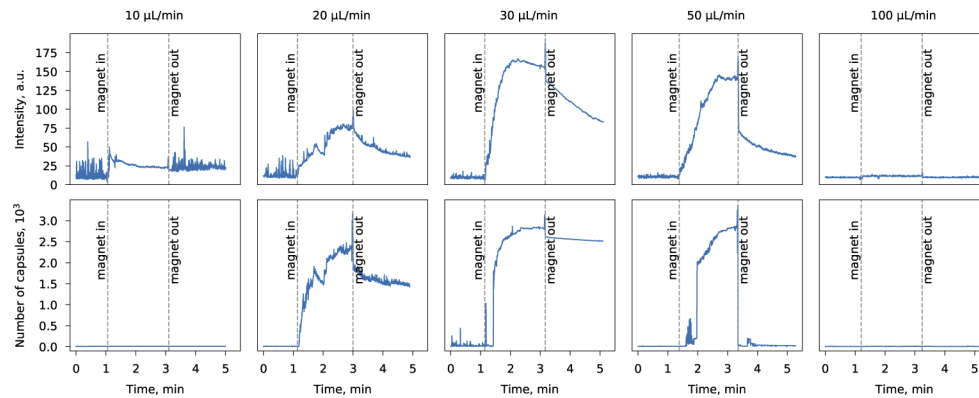


Fig. 2. Average fluorescence intensity with the excitation by 488 nm laser and 505–555 nm detection range, measured in the lightsheet region of the flow cell at different flow rates of microcapsule suspension (top row) and the number of capsules, calculated from the fluorescence imaging data (bottom row).

At the lowest flow rate of 10 $\mu\text{L}/\text{min}$, the microcapsules did not accumulate significantly under the magnetic field influence. The average fluorescence intensity values upon the application of a magnet were close to the background baseline and did not exceed 50 a.u. (Fig. 2, top row, 10 $\mu\text{L}/\text{min}$). The number of capsules also did not show significant changes under the magnetic field influence (Fig. 2, bottom row, 10 $\mu\text{L}/\text{min}$). It was probably caused by a low number of capsules passing through the flow cell during the accumulation period. With the increase in the flow rate to 20 $\mu\text{L}/\text{min}$, the accumulation increased, but this process was relatively slow. It can be seen from the increase in the average fluorescence intensity (Fig. 2, top row, 20 $\mu\text{L}/\text{min}$) and the number of capsules detected in the lightsheet area per second (Fig. 2, bottom row, 20 $\mu\text{L}/\text{min}$). Both curves had a characteristic slope before reaching the saturation region. The accumulation at 30 and 50 $\mu\text{L}/\text{min}$ rate showed the same behavior: when the magnet was applied to the flow cell, we could see a sharp increase of signal intensity (Fig. 2, top row, 30 and 50 $\mu\text{L}/\text{min}$) and a number of

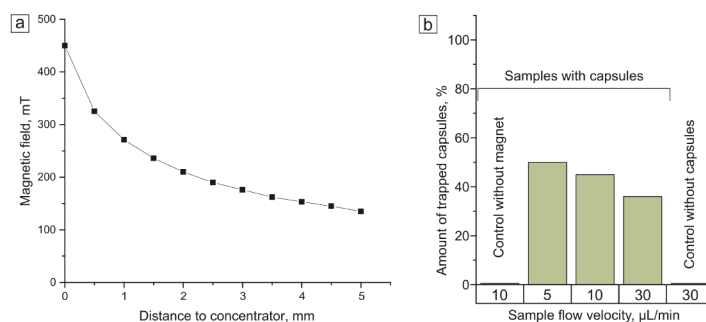


Fig. 3. Distribution of magnetic field near the magnet concentrator (a), and the efficiency of magnetic microcapsule separation from flowing blood *in vitro* (b).

capsules detected per sec (Fig. 2, bottom row, 30 and 50 $\mu\text{L}/\text{min}$) followed by a saturation region. The magnet removal led to the immediate decrease in the fluorescence intensity and the number of capsules, respectively. However, the microcapsule accumulation happened 1.5 times faster at 30 $\mu\text{L}/\text{min}$ rate if compared with 50 $\mu\text{L}/\text{min}$. This can be caused by washing of magnetically captured objects by multiple collisions with microcapsules flowing through the channel. After removing the magnet, most of the adsorbed microcapsules were washed out. At 100 $\mu\text{L}/\text{min}$ rate, nothing was captured by the magnet, since the impulse of the flowing microcapsules colliding with the captured ones presumably exceeded the force holding the microcapsules in the trap (Fig. 2, 100 $\mu\text{L}/\text{min}$).

Whether an object will be held in a region of a strong magnetic field is determined by the balance of forces acting on it. The object is held in place by the magnetic field and adhesion from adjacent objects. It should also be noted that the residual magnetization of objects and adhesion forces continue to operate even some time after the magnet removal from the flow cell. However, the object can be knocked out of the magnetic trap due to the impact of the fluid flow itself and collisions with other objects carried by the flow. Moreover, the accumulated volume of capsules makes the stream alongside the magnetic concentrator more narrow, therefore increasing flow speed in this area and the washing effect of the stream.

3.2. Magnetic microcapsule separation from the whole blood *in vitro*

The efficient capture of magnetic objects *in vivo* will require to separate them from the flowing blood, which contains about $8\text{--}9 \times 10^9$ erythrocytes per mL as well as leukocytes, thrombocytes, proteins, ions of Ca^{2+} , Mg^{2+} , Na^{+} , etc. The high concentration of these objects in the blood can affect the ability and efficiency of the separation of individual magnetic capsules, as they must overcome mechanical tension and impulses from multiple collisions with other objects when crossing the region of the strongest magnetic field.

Furthermore, *in vivo* procedures place some restrictions on the size of used objects to ensure safety of their circulation in the bloodstream. As it was shown in our previous paper [38], micron-sized polymeric capsules do not disrupt the blood flow, and the organism can adapt to the appearance of the carriers in the blood as well as their accumulation in blood vessels and organs. This makes the magnetic capsules of micron size a relevant, safe, and preferable choice for further *in vivo* experiments.

The testing of the ability to efficiently separate magnetic microcapsules from the blood was required before we started *in vivo* experiments. We evaluated the dependence of microcapsule capture efficiency by the magnetic field on the flow rate in the cytometer flow cell *in vitro*. The magnetic objects were represented by the microcapsules used above. The whole rat blood, diluted 3:1 with PBS, represented the control sample without any microcapsules. For other samples,

the whole blood was diluted with microcapsule suspension in PBS in the same ratio. The final concentration was about 14.65×10^6 carriers per mL. The separation ability was tested at the suspension flow rates: 5, 10, and 30 $\mu\text{L}/\text{min}$. The amount of captured carriers was assessed using the imaging flow cytometer Amnis ImageStream X Mk II (Fig. 3(b)).

Therefore, the efficiency of microcapsule capture from the blood slightly decreases with the increase in the sample flow rate (Fig. 3(b)). For example, at the 30 $\mu\text{L}/\text{min}$ 35.6% of carriers was trapped from the initial amount compared to the 44.6% at 5 $\mu\text{L}/\text{min}$ rate.

3.3. Experiment with the animal model

The evaluation of magnetic capsules' capture efficiency *in vivo* was performed on the rat model. Blood vessels of a white rat were connected to the cytometer flow cell by the polyethylene catheters inserted into the femoral artery and vein of the rat's hind paw. 1.1×10^7 capsules suspended in 20 μL of physiological salt solution were injected into the carotid artery (Fig. 4(a, b)). The injection was performed through the catheter, accompanied by heparin injection to prevent blood coagulation.

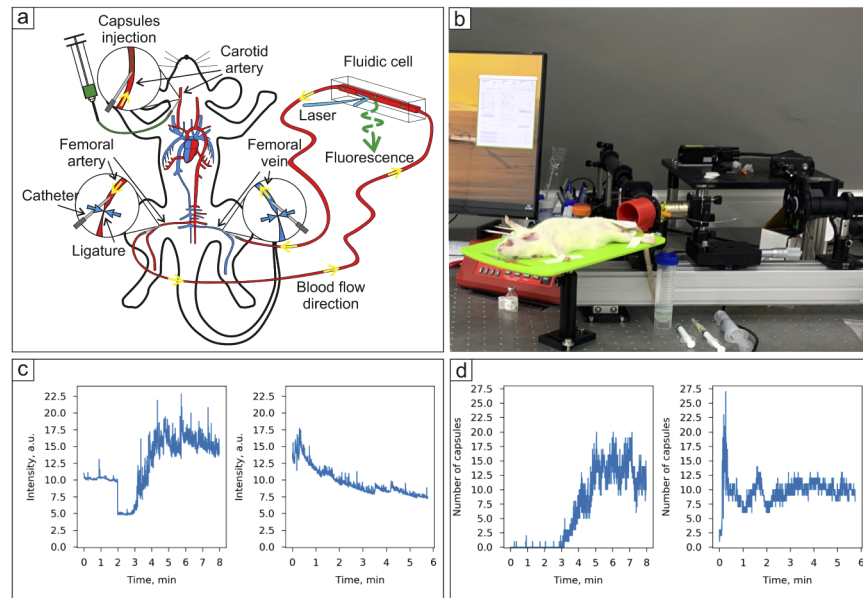


Fig. 4. Separation of magnetic microcapsules from rat blood *in vivo*. Scheme of the experiment (a); the photo of the rat connected to the system (b); detection of microcapsules in rat bloodstream (c, d), where (c) represents average fluorescence intensity under 488 nm laser excitation and 505–555 nm detection range in lightsheet area, (d) represents the number of capsules estimated from the detected fluorescent signal. Left plots in (c, d) correspond to average fluorescence intensity / number of capsules without a magnet; right ones represent the flow with magnetic separation downstream of the magnet.

Figure 4 represents the carrier circulation dynamics in the rat blood flow and a decrease in microcapsule concentration in the bloodstream due to both systemic filtration by internal organs (in particular, by the liver) and magnet-induced accumulation of capsules in the flow cell. Until the 120th sec (Fig. 4(c) (left)) we could see the autofluorescence of erythrocytes in the flow channel. The 120th sec point corresponds to the injection of microcapsules into the blood flow (the sharp decay of the signal could be caused both by the artifacts induced by the interaction between the rat and the optical system, and the optical clearing of the blood due to the

decrease in erythrocytes number after its dilution by PBS). We could see the beginning of the carriers' circulation several seconds after microcapsule suspension injection into the bloodstream in the absence of a magnetic field (Fig. 4(c) (left)). Microcapsules were circulating in the blood circulatory system for a significant period of time (20–30 min and more). According to our previous data [37], the circulation time of 3–5 μm microcapsules (versus 1.34 μm in the current study) was much shorter, and the number of microcapsules in the blood rapidly decreased within the first 3 min. After the magnet was brought in (the 20th sec in Fig. 4(c) (right)), the number of carriers in the blood flow downstream of the magnet decreased relative to the initial value, corresponding to the first minutes of recording. We estimated the amount of fluorescent material in the channel and converted it into a number of capsules (Fig. 4(d)).

Doppler optical coherence tomography (DOCT) cross-sections of the bypass polymer tube, artery, and vein are presented in Fig. 5. Phase unwrapping was done prior to the calculation of the blood flow velocity values to obtain correct results (see Supplementary Note 2 and Fig. S2 in Supplement 1). Due to the turbulent nature of arterial blood flow, it was impossible to apply the phase unwrapping algorithm; therefore the average phase difference over the entire vessel was used to calculate the values of the arterial blood flow velocity. According to the DOCT data, capsule injection in the blood-vascular system caused an insignificant slowdown of the arterial and vein blood flow with subsequent recovery to the initial values. Magnetic capture of microcapsules did not provide any impact on the blood flow velocity, which indirectly indicates the absence of vessel embolism and thrombosis. The speed of blood flow inside the capillary flow cell was 1.4 ± 0.8 cm/s. The speed of blood was 2.1 ± 1.2 cm/s inside the artery and 1.1 ± 0.6 cm/s inside the vein. Taking into account the vessels' diameters, that were ~ 0.2 mm for artery, ~ 0.35 mm for vein, and 0.28 mm inner diameter of the polymer tube, the flow rates were ~ 0.04 mL/min in artery, ~ 0.06 mL/min in vein, and 0.05 mL/min in the flow cytometry system. These flow rates are nearly identical as they are all connected and should have approximately the same volumetric flow rate.

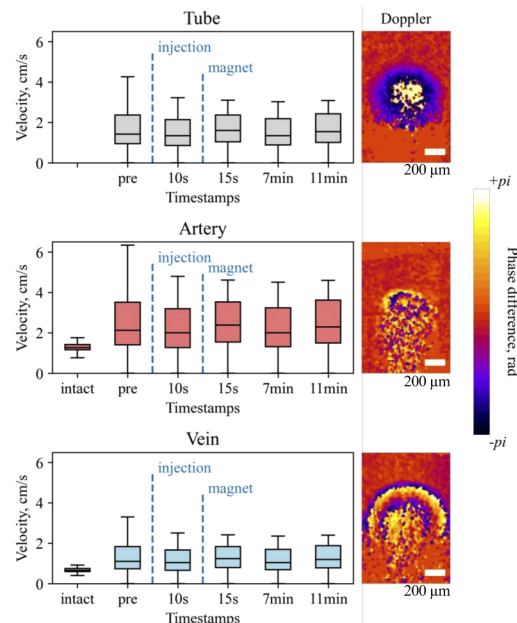


Fig. 5. Blood flow velocity measurements in the catheter, artery, and vein by the means of DOCT. Capsules injection and beginning of magnetic trapping are indicated by vertical lines. Examples of Doppler phase images shown at the right column.

Magnetic trapping of microcapsules was carried out for 10 min by the 0.3 T magnet, followed by removal of the magnet and washing the trapped microcapsules into an outer tube by several rinses with PBS. The number of magnetically-trapped capsules was independently measured using the imaging flow cytometer Amnis ImageStream X Mk II. Fluorescence signals of FITC-labeled microcapsules and autofluorescence intensity of blood erythrocytes are well spectrally-separated [37,38].

The microcapsules' collection was carried out for a fixed sample volume, and then the total number of retrieved carriers was calculated (Table 1). The initial capsule concentration in the approximate whole volume of rat blood (15 mL) was around 7.81×10^5 capsules per mL. During flow cytometry measurements, 20 μL of the whole blood was analyzed. We found that the number of capsules in the sample after magnetic capture was around 25 times higher (3.97×10^5 capsules per 20 μL) than the calculated number of capsules contained in a similar blood volume (0.15×10^5 capsules per 20 μL). Moreover, the actual number of circulating microcapsules was less than the calculated one, since we did not take into account the filtration and accumulation of microcapsules in internal organs (for instance, lungs, kidneys, liver) during the experiment. This indicates the possibility of using the developed magnetic separator for efficient capture of capsules.

Table 1. The calculation of microcapsule separation efficiency from blood *in vivo*

Rat blood volume, mL	Amount of capsules injected, obj	Microcapsule concentration in blood, obj/mL	Amount of circulating capsules (in tube volume), obj	Amount of trapped capsules, obj
15	11 720 400	781 360	15 627	397 367

Fluorescence images of microcapsules before and after their injection to the blood flow showed the absence of significant differences between them, except for the higher aggregation degree of capsules captured from the whole blood (Fig. 6(c, d)) in comparison with the water suspension (Fig. 6(a, b)). This effect can be caused by the close interaction between the capsule shells during their accumulation in the region of a strong magnetic field and the interaction of the capsules with various blood proteins, which can play the role of binding molecules [37].

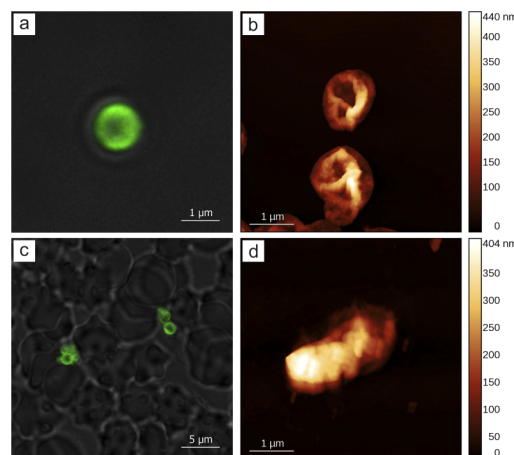


Fig. 6. Characterization of the microcapsules. CLSM (a, c) and AFM (b, d) images of initial water suspension of capsules (a, b) and capsules captured from the bloodstream (c, d).

AFM images of capsules after the experiment showed slightly decreased thickness of the shell (50–56 nm of double-layer shell thickness against the 70–80 nm before the injection) probably due to some interaction of biodegradable microcapsule shell with the whole blood. We could also see the presence of some debris on the surface of microcapsule shells which could be adsorbed prior to extraction or as a part of the extracted suspension.

Thus, we have developed a new type of *in vivo* flow cytometry system. It allows objects to be measured and imaged in undiluted blood; it allows the long-term *in vivo* experiments with the total blood volume of an animal to be performed without taking blood samples; and it allows objects to be retrieved from the bloodstream. The developed technique is definitely more invasive compared to systems based on photoacoustics or diffuse fluorescence. But an external flow cell connected to large blood vessels gives us opportunities not available in other systems.

In this study, we demonstrated some basic set of features: counting objects for an experiment with an artificial CTC phantom; continuously extracting objects from animal whole blood; determining the characteristics of objects extracted from the bloodstream, which was not possible before. It can be extended to address more specific challenges in biomedical research, for instance, providing simultaneous measurements and imaging in multiple fluorescent channels, or separating and sorting objects on demand (based on images if needed). So, we hope that we have developed a useful new tool that expands the ability to work with rare objects in the bloodstream and, thus, allows us to better understand some of the basic biological processes in the body.

4. Conclusion

The developed SPIM-based imaging flow cytometry system is capable of detecting objects in whole blood both *in vivo* and *in vitro*, followed by magnetic retrieval. Two object counting methods were applied to detect objects on the video stream from the sCMOS camera. The first one is based on total fluorescence in the lightsheet plane and is similar to the data analysis in traditional flow cytometry based on point detectors. The second one is based on the object separation from the image background with subsequent object size evaluation. The first method works well if the concentration of objects is very high and they become indistinguishable in the camera images. The second one works well for sparse separated objects, or when the number of objects in the aggregate can be evaluated by its size. Effective magnetic separation of objects from the PBS buffer stream has been shown with 0.3 T magnetic field near the tip of the field concentrator at a flow rate of 20–50 $\mu\text{L}/\text{min}$. The developed system allowed us to monitor fluorescently-labeled microcapsules inside the flow cell shunting two large blood vessels of a rat limb after their injection into the carotid artery. The speed of blood flow measured by the DOCT was 1.4 ± 0.8 cm/s inside the shunting polymer tube; 2.1 ± 1.2 and 1.1 ± 0.6 cm/s inside the artery and the vein, respectively. We have shown the separation of about 4×10^5 microcapsules *in vivo* from blood by a 0.3 T permanent magnet with a concentrator. The extracted objects were measured afterward by imaging flow cytometry, CLSM, and AFM methods. An unexpected effect of reducing the microcapsule shell thickness after passing through the bloodstream was found along with the adsorption of a large amount of debris on it.

Funding

Russian Science Foundation (18-19-00354).

Acknowledgments

The study was supported by Russian Science Foundation (project no. 18-19-00354).

Disclosures

The authors declare no conflicts of interest.

See [Supplement 1](#) for supporting content.

References

1. C. Alix-Panabières and K. Pantel, "Clinical applications of circulating tumor cells and circulating tumor DNA as liquid biopsy," *Cancer Discov.* **6**(5), 479–491 (2016).
2. O. A. Sindeeva, R. A. Verkhovskii, M. Sarimollaoglu, G. A. Afanaseva, A. S. Fedonnikov, E. Y. Osintsev, E. N. Kurochkina, D. A. Gorin, S. M. Deyev, V. P. Zharov, and E. I. Galanzha, "New frontiers in diagnosis and therapy of circulating tumor markers in cerebrospinal fluid *in vitro* and *in vivo*," *Cells* **8**(10), 1195 (2019).
3. M. Harz, M. Kiehnopf, S. Stöckel, P. Rösch, E. Straube, T. Deufel, and J. Popp, "Direct analysis of clinical relevant single bacterial cells from cerebrospinal fluid during bacterial meningitis by means of micro-Raman spectroscopy," *J. Biophotonics* **2**(1-2), 70–80 (2009).
4. C. Cai, K. A. Carey, D. A. Nedosekin, Y. A. Menyaev, M. Sarimollaoglu, E. I. Galanzha, J. S. Stumhofer, and V. P. Zharov, "In vivo photoacoustic flow cytometry for early malaria diagnosis," *Cytom. Part A* **89**(6), 531–542 (2016).
5. L. Lind, "Circulating markers of inflammation and atherosclerosis," *Atherosclerosis* **169**(2), 203–214 (2003).
6. E. I. Galanzha, M. Sarimollaoglu, D. A. Nedosekin, S. G. Keyrouz, J. L. Mehta, and V. P. Zharov, "In vivo flow cytometry of circulating clots using negative photothermal and photoacoustic contrasts," *Cytom. Part A* **79A**(10), 814–824 (2011).
7. J. G. Moreno, S. O'Hara, S. Gross, G. Doyle, H. Fritsche, L. G. Gomella, and L. W. Terstappen, "Changes in circulating carcinoma cells in patients with metastatic prostate cancer correlate with disease status," *Urology* **58**(3), 386–392 (2001).
8. L. Yang, J. C. Lang, P. Balasubramanian, K. R. Jatana, D. Schuller, A. Agrawal, M. Zborowski, and J. J. Chalmers, "Optimization of an enrichment process for circulating tumor cells from the blood of head and neck cancer patients through depletion of normal cells," *Biotechnol. Bioeng.* **102**(2), 521–534 (2009).
9. I.-F. Cheng, H.-C. Chang, T.-Y. Chen, C. Hu, and F.-L. Yang, "Rapid (<5 min) identification of pathogen in human blood by electrokinetic concentration and surface-enhanced Raman spectroscopy," *Sci. Rep.* **3**(1), 2365 (2013).
10. X. Tan, R. Patil, P. Bartosik, J. M. Runnels, C. P. Lin, and M. Niedre, "In Vivo flow cytometry of extremely rare circulating cells," *Sci. Rep.* **9**(1), 3366 (2019).
11. R. Patil, X. Tan, P. Bartosik, A. Detappe, J. M. Runnels, I. Ghobrial, C. P. Lin, and M. Niedre, "Fluorescence monitoring of rare circulating tumor cell and cluster dissemination in a multiple myeloma xenograft model *in vivo*," *J. Biomed. Opt.* **24**(8), 1–11 (2019).
12. M. Juratli, M. Sarimollaoglu, D. Nedosekin, A. Melerzanov, V. Zharov, and E. Galanzha, "Dynamic Fluctuation of circulating tumor cells during cancer progression," *Cancers* **6**(1), 128–142 (2014).
13. A. L. Williams, J. E. Fitzgerald, F. Ivich, E. D. Sontag, and M. Niedre, "Short-term circulating tumor cell dynamics in mouse xenograft models and implications for liquid biopsy," *Front. Oncol.* **10**, 601085 (2020).
14. R. Liu, C. Wang, C. Hu, X. Wang, and X. Wei, "In vivo, label-free, and noninvasive detection of melanoma metastasis by photoacoustic flow cytometry," in *Biophotonics and Immune Responses IX*, vol. 8944 W. R. Chen, ed., International Society for Optics and Photonics (SPIE, 2014), pp. 121–127.
15. E. I. Galanzha, Y. A. Menyaev, A. C. Yadem, M. Sarimollaoglu, M. A. Juratli, D. A. Nedosekin, S. R. Foster, A. Jamshidi-Parsian, E. R. Siegel, I. Makhoul, L. F. Hutchins, J. Y. Suen, and V. P. Zharov, "In vivo liquid biopsy using Cytophone platform for photoacoustic detection of circulating tumor cells in patients with melanoma," *Sci. Transl. Med.* **11**(496), eaat5857 (2019).
16. M. A. Juratli, Y. A. Menyaev, M. Sarimollaoglu, E. R. Siegel, D. A. Nedosekin, J. Y. Suen, A. V. Melerzanov, T. A. Juratli, E. I. Galanzha, and V. P. Zharov, "Real-Time Label-Free Embolus Detection Using In Vivo Photoacoustic Flow Cytometry," *PLoS One* **11**(5), e0156269 (2016).
17. V. P. Zharov, E. I. Galanzha, E. V. Shashkov, J.-W. Kim, N. G. Khlebtsov, and V. V. Tuchin, "Photoacoustic flow cytometry: principle and application for real-time detection of circulating single nanoparticles, pathogens, and contrast dyes *in vivo*," *J. Biomed. Opt.* **12**(5), 051503 (2007).
18. V. Pera, X. Tan, J. Runnels, N. Sardesai, C. P. Lin, and M. Niedre, "Diffuse fluorescence fiber probe for *in vivo* detection of circulating cells," *J. Biomed. Opt.* **22**(3), 037004 (2017).
19. X. Cao, C. Yao, S. Jiang, J. Gunn, A. C. Van Namen, P. Bruza, and B. W. Pogue, "Time-gated luminescence imaging for background free *in vivo* tracking of single circulating tumor cells," *Opt. Lett.* **45**(13), 3761–3764 (2020).
20. E. J. Gualda, H. Pereira, T. Vale, M. F. Estrada, C. Brito, and N. Moreno, "SPIM-fluid: open source light-sheet based platform for high-throughput imaging," *Biomed. Opt. Express* **6**(11), 4447–4456 (2015).
21. H. Yamada, A. Hirotsu, D. Yamashita, O. Yasuhiko, T. Yamauchi, T. Kayou, H. Suzuki, S. Okazaki, H. Kikuchi, H. Takeuchi, and Y. Ueda, "Label-free imaging flow cytometer for analyzing large cell populations by line-field quantitative phase microscopy with digital refocusing," *Biomed. Opt. Express* **11**(4), 2213–2223 (2020).
22. Y. Han, R. Tang, Y. Gu, A. C. Zhang, W. Cai, V. Castor, S. H. Cho, W. Alaynick, and Y.-H. Lo, "Cameraless high-throughput three-dimensional imaging flow cytometry," *Optica* **6**(10), 1297–1304 (2019).
23. H. Mikami, M. Kawaguchi, C.-J. Huang, H. Matsumura, T. Sugimura, K. Huang, C. Lei, S. Ueno, T. Miura, T. Ito, K. Nagasawa, T. Maeno, H. Watarai, M. Yamagishi, S. Uemura, S. Ohnuki, Y. Ohya, H. Kurokawa, S. Matsusaka, C.-W.

- Sun, Y. Ozeki, and K. Goda, "Virtual-freezing fluorescence imaging flow cytometry," *Nat. Commun.* **11**(1), 1162 (2020).
24. B. Zebli, A. S. Susha, G. B. Sukhorukov, A. L. Rogach, and W. J. Parak, "Magnetic targeting and cellular uptake of polymer microcapsules simultaneously functionalized with magnetic and luminescent nanocrystals," *Langmuir* **21**(10), 4262–4265 (2005).
 25. D. V. Voronin, O. A. Sindeeva, M. A. Kurochkin, O. Mayorova, I. V. Fedosov, O. Semyachkina-Glushkovskaya, D. A. Gorin, V. V. Tuchin, and G. B. Sukhorukov, "In vitro and in vivo visualization and trapping of fluorescent magnetic microcapsules in a bloodstream," *ACS Appl. Mater. Interfaces* **9**(8), 6885–6893 (2017).
 26. O. A. Mayorova, O. A. Sindeeva, M. V. Lomova, O. I. Gusliakova, Y. V. Tarakanchikova, E. V. Tyutyayev, S. I. Pinyayev, O. A. Kulikov, S. V. German, N. A. Pyataev, D. A. Gorin, and G. B. Sukhorukov, "Endovascular addressing improves the effectiveness of magnetic targeting of drug carrier. Comparison with the conventional administration method," *Nanomedicine: Nanotechnology, Biol. Medicine* **28**, 102184 (2020).
 27. F. Paul, S. Roath, D. Melville, D. Warhurst, and J. Osisanya, "Separation of malaria-infected erythrocytes from whole blood: use of a selective high-gradient magnetic separation technique," *The Lancet* **318**(8237), 70–71 (1981).
 28. C. S. Owen and N. L. Sykes, "Magnetic labeling and cell sorting," *J. Immunol. Methods* **73**(1), 41–48 (1984).
 29. Y. Haik, V. Pai, and C.-J. Chen, "Development of magnetic device for cell separation," *J. Magn. Magn. Mater.* **194**(1-3), 254–261 (1999).
 30. D. W. Inglis, R. Riehn, J. C. Sturm, and R. H. Austin, "Microfluidic high gradient magnetic cell separation," *J. Appl. Phys.* **99**(8), 08K101 (2006).
 31. G. Frodsham and Q. A. Pankhurst, "Biomedical applications of high gradient magnetic separation: progress towards therapeutic haemofiltration," *Biomed. Eng. / Biomedizinische Tech.* **60**(5), 393–404 (2015).
 32. R. Massart, "Preparation of aqueous magnetic liquids in alkaline and acidic media," *IEEE Trans. Magn.* **17**(2), 1247–1248 (1981).
 33. S. V. German, O. A. Inozemtseva, A. V. Markin, K. Metvalli, G. B. Khomutov, and D. A. Gorin, "Synthesis of magnetite hydrosols in inert atmosphere," *Colloid J.* **75**(4), 483–486 (2013).
 34. D. B. Trushina, T. V. Bukreeva, and M. N. Antipina, "Size-controlled synthesis of vaterite calcium carbonate by the mixing method: aiming for nanosized particles," *Cryst. Growth & Des.* **16**(3), 1311–1319 (2016).
 35. I. of Laboratory Animal Resources (US). Committee on Care and U. of Laboratory Animals, *Guide for the care and use of laboratory animals*, 86 (US Department of Health and Human Services, Public Health Service, National Institute of Health, 1986).
 36. D. Nečas and P. Klapetek, "Gwyddion: an open-source software for SPM data analysis," *Open Phys.* **10**(1), 181–188 (2012).
 37. R. Verkhovskii, A. Kozlova, A. Ermakov, E. Lengert, and D. Bratashov, "Investigation of polyelectrolyte microcapsule aggregation in human blood," in *Saratov Fall Meeting 2018: Optical and Nano-Technologies for Biology and Medicine*, V. V. Tuchin and E. A. Genina, eds. (SPIE, 2019), p. 85.
 38. O. A. Sindeeva, R. A. Verkhovskii, A. S. Abdurashitov, D. V. Voronin, O. I. Gusliakova, A. A. Kozlova, O. A. Mayorova, A. V. Ermakov, E. V. Lengert, N. A. Navolokin, V. V. Tuchin, D. A. Gorin, G. B. Sukhorukov, and D. N. Bratashov, "Effect of systemic polyelectrolyte microcapsule administration on the blood flow dynamics of vital organs," *ACS Biomater. Sci. Eng.* **6**(1), 389–397 (2020).
 39. L. J. De Cock, S. De Koker, B. G. De Geest, J. Grooten, C. Vervaet, J. P. Remon, G. B. Sukhorukov, and M. N. Antipina, "Polymeric multilayer capsules in drug delivery," *Angewandte Chemie Int. Ed.* **49**(39), 6954–6973 (2010).
 40. S. Carregal-Romero, M. Ochs, and W. J. Parak, "Nanoparticle-functionalized microcapsules for in vitro delivery and sensing," *Nanophotonics* **1**(2), 171–180 (2012).
 41. I. Y. Stetsiura, A. Yashchenok, A. Masic, E. V. Lyubin, O. A. Inozemtseva, M. G. Drozdova, E. A. Markvichova, B. N. Khlebtsov, A. A. Fedyanin, G. B. Sukhorukov, D. A. Gorin, and D. Volodkin, "Composite SERS-based satellites navigated by optical tweezers for single cell analysis," *The Analyst* **140**(15), 4981–4986 (2015).
 42. A. M. Yashchenok, J. Jose, P. Trochet, G. B. Sukhorukov, and D. A. Gorin, "Multifunctional polyelectrolyte microcapsules as a contrast agent for photoacoustic imaging in blood," *J. Biophotonics* **9**(8), 792–799 (2016).
 43. M. V. Novoselova, D. N. Bratashov, M. Sarimollaoglu, D. A. Nedosekin, W. Harrington, A. Watts, M. Han, B. N. Khlebtsov, E. I. Galanzha, D. A. Gorin, and V. P. Zharov, "Photoacoustic and fluorescent effects in multilayer plasmon-dye interfaces," *J. Biophotonics* **12**(4), e201800265 (2019).